Bipolar Thermoelectrical Transport of SnSe Nanoplate in Low Temperature *

Li-Yan Zhou(周利艳)[1,2], Qi Zheng(郑琦)[1,2], Li-Hong Bao(鲍丽宏)[1,2], Wen-Jie Liang(梁文杰)[1,2,3]**

[1]*Beijing National Center for Condensed Matter Physics, Beijing Key Laboratory for Nanomaterials and Nanodevices, Institute of Physics, Chinese Academy of Sciences, Beijing 100190*

[2]*CAS Center of Excellence in Topological Quantum Computation and School of Physical Sciences, University of Chinese Academy of Sciences, Beijing 100190*

[3]*Songshan Lake Materials Laboratory, Dongguan 523808*

(Received 12 October 2019)

Bulk SnSe is an excellent thermoelectrical material with the highest figure-of-merit value of $ZT = 2.8$, making it promising in applications. Temperature-dependent electrical and thermoelectrical properties of SnSe nanoplates are studied at low temperature. Conductivity drops and rises again as temperature is lowered. The Seebeck coefficient is positive at room temperature and becomes negative at low temperature. The change of the sign of the Seebeck coefficient indicates influence of bipolar transport of the semiconductive SnSe nanoplate. The bipolar transport is caused by the Fermi energy changing with temperature due to different contributions from donors and acceptors at different temperatures.

PACS: 73.50.Lw, 73.50.Gr, 73.63.Bd, 85.80.Fi

DOI: 10.1088/0256-307X/37/1/017301

Thermoelectricity as a promising way of providing eco-friendly energy generation is increasingly attracting attention. Conventionally, it requires solid state material incorporating heavy element for efficient energy harvesting in thermoelectric modules.[1] The energy conversion efficiency is characterized by figure-of-merit $ZT = \frac{\sigma S^2 T}{\kappa_l + \kappa_e}$, where σ is electrical conductivity, S is Seebeck coefficient, T is absolute temperature, κ_l and κ_e are the lattice and electron thermal conductivity, respectively.[2,3]

So far, the energy conversion efficiency is very low, and higher ZT is needed to improve the energy conversion efficiency. Generally, there are several ways to improve ZT of thermoelectrical materials: (1) using nano-materials to enhance the Seebeck coefficient due to the quantum confinement and to reduce thermal conductivity due to the surface-phonon scattering,[4–8] (2) imploring materials with complex structures to reduce lattice thermal conductivity,[9–12] (3) increasing spin-dependent Seebeck coefficient by introducing magnetic groups as predicted in theory.[13]

Materials with ZT above 3 are required to be comparable with main stream energy generation methods.[14–17] Recently, SnSe rises to be a promising thermoelectric material with ZT close to 3.[18] Thus, SnSe is among the most promising thermoelectrical materials,[19–21] and has been a hot spot since it is first reported as a thermoelectrical material.[22–24]

The nano-structured thermoelectrical materials have made great progress[25–27] as predicted in theory, indicating a promising way to get better thermoelectrical properties. In this Letter, we investigate electrical and thermoelectrical properties of SnSe nanoplates. Our results show a carrier type change from hole to electron while the temperature is changed, based on both electrical and thermoelectrical measurements. The nonmonotonic temperature dependence and sign change of electrical conductivity and Seebeck coefficient show a bipolar transport in our SnSe nanoplates. The bipolar transport of SnSe has been predicted in theory[28] and discussed in experimental results at high temperature (~700 K), but has never been observed at low temperature before. We provide, for the first time, experimental evidence of bipolar transport properties of SnSe below room temperature, and experimentally investigate the sign change of Seebeck coefficient.

Our SnSe nanoplates were synthesized using the chemical vapor deposition (CVD) method[29] with different sizes growing vertically on the SiO_2/Si substrate, as shown in Fig. 1(a). Under an optical microscope, the bright ones are those that have fallen on the substrate after growth and the black ones are the upstanding SnSe nanoplates. The inset is a scanning electron microscope (SEM) image of the upstanding SnSe nanoplates. The surface tension makes the

*Supported by the National Basic Research Program of China under Grant No. 2016YFA0200800, the Strategic Priority Research Program of Chinese Academy of Sciences under Grant No. XDB30000000, the Strategic Priority Research Program of Chinese Academy of Sciences under Grant No. XDB07030100, the Sinopec Innovation Scheme (A-381), and the Rise.Sinopec Fund under Grant No. 10010104-18-ZC0609-0003.

**Correspondence author. Email: wjliang@iphy.ac.cn

© 2020 Chinese Physical Society and IOP Publishing Ltd

thin nanoplate curl, as shown. However, when the upstanding sample is pulled down by an external force, it lies down and sticks to the substrate perfectly and flat. In our experiment, the samples of interest are picked from the upstanding nanoplates with desired thickness by a microtip.

An atomic force microscope (AFM) was used to character the surface morphology of the sample. Figure 1(b) shows a typical AFM image of an as-synthesized SnSe nanoplate. The sample is flat and uniform, with the thickness of 92 nm. The thickness of the synthesized samples ranges from dozens to several hundreds of nanometer.

To verify that the as-synthesized samples are SnSe single crystal, a Cs-corrected transmission electron microscope (Cs-corrected TEM) was used to characterize the structure of the sample. Figures 1(c) and 1(d) are the Cs-corrected TEM image and the selected area electron diffraction (SAED) pattern of SnSe nanoplates. The 011 and $01\bar{1}$ planes are clearly resolved with lattice spacing around 3 Å and our nanoplates are in *bc* plane, vertical to the *a* axis of SnSe. In addition, the SAED of SnSe shows the perfect single crystalline of our nanoplates with the orthorhombic phase (space group *Pnma*).[29]

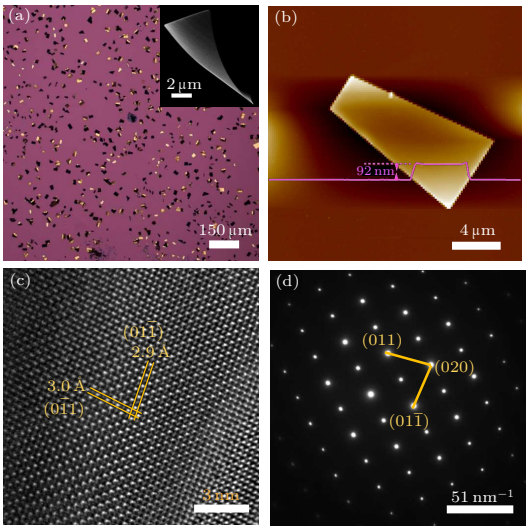

Fig. 1. (a) The optical image of the synthesized SnSe nanoplate. Inset: the SEM image of an upstanding SnSe sample. (b) The AFM image of a SnSe nanoplate. (c) The Cs-corrected TEM image. (d) The SAED pattern of SnSe.

To obtain the thermoelectric properties of the SnSe nanoplate, a micro-device[30,31] was utilized, as shown in Fig. 2(a). The SnSe nanoplate was picked up using a sharp probe with the aid of micro-manipulator,[32] then dry transferred onto a new clean SiO_2/Si substrate with markers on it. The markers are used to locate the sample with the help of an optical microscope. After the sample was coated with PMMA, electron beam lithography (EBL) was utilized to make the electrodes' pattern, followed by development of the generated pattern. Ni/Au[33] were then deposited using thermal evaporation, and the lift-off processes was followed to complete the device.

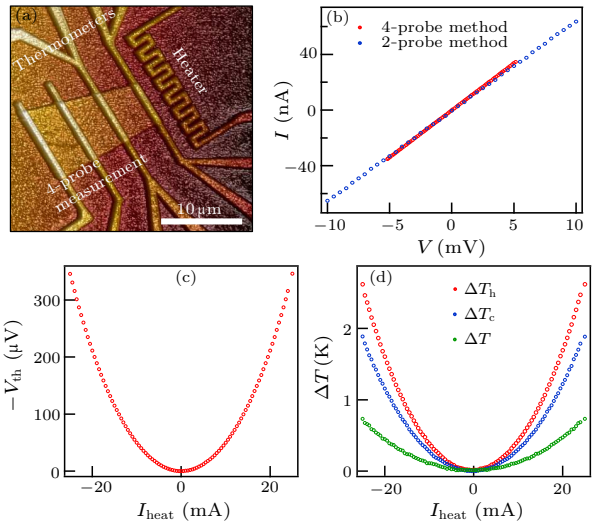

Fig. 2. (a) AFM image of the fabricated thermoelectric device. (b) *I*–*V* curves from the two-probe electrical measurement method (blue symbol) and the four-probe measurement method (red symbol). (c) Thermovoltage as a function of heating current. (d) ΔT_h (red symbol), ΔT_c (blue symbol) and ΔT (green symbol) versus heating current.

The thermoelectric device consists of a heater, two thermometers and two other electrodes. Four-probe electrical measurement was used to obtain the intrinsic electric conductivity, ruling out the contact resistance. The thickness of the sample shown in Fig. 2 is 113 nm. The *I*–*V* curves are presented in Fig. 2(b). The blue dots are the two-probe results, and the red dots are the four-probe results. These two curves form straight lines and almost coincide with each other, with a negligible contact resistance of about 4%. This indicates that the contact between the SnSe and Ni/Au is good. The measured conductivity is 0.3 S/cm, smaller than bulk SnSe. This may be caused by surface scattering and impurity scattering.

We also measured electrical properties of several SnSe nanoplates with the van der Pauw method for comparison, making sure that the above fabrication method did not alter sample's intrinsic properties. The results show that the conductivities of SnSe nanoplates are about 0.1–6 S/cm with the thickness of about 80–140 nm, which is comparable with 0.3 S/m of the thermoelectrical device in the thickness of 113 nm.

Figures 2(c) and 2(d) show the thermoelectrical measurements. An AC method was used to obtain the thermoelectric properties.[34] When a DC current was

applied on the heater, the generated heat on the heater would disperse across the measured sample, generating a temperature gradient inside the SnSe nanoplate, which can be monitored by the resistant changes of the two thermometers vertical to temperature gradient. AC voltages and currents were applied to the thermometers to accurately measure the resistance. The thermovoltage generated inside the nanoplate can also be picked up by the two thermometers. Figure 2(c) is the negative thermovoltage ($-V_{\rm th}$) as a function of heating current ($I_{\rm heat}$), showing a parabolic relationship. Figure 2(d) is the temperature increase of the hot end ($\Delta T_{\rm h}$) and the cold end ($\Delta T_{\rm c}$) as well as the temperature difference between the hot end and cold end ($\Delta T = \Delta T_{\rm h} - \Delta T_{\rm c}$) as a function of heating current, also showing a parabolic relationship. The parabolic dependence to the current indicates that the thermovoltage and temperature difference are linear dependent on heating power. The Seebeck can be obtained by the division of thermovoltage and temperature difference between the same two thermometers ($S = -\frac{\Delta V_{\rm th}}{\Delta T}$). The Seebeck of the device shown in Fig. 2(a) is 472 μV/K. The positive value indicates the p-type semiconductor at room temperature. The Seebeck coefficient of our SnSe nanoplate is higher than hole doped bulk SnSe (∼160 μV/K) while comparable to that of undoped (intrinsic) bulk SnSe (∼500 μV/K).

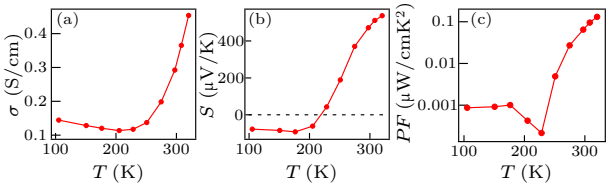

Fig. 3. (a) Electrical conductivity as a function of temperature between 100 K and 320 K. (b) Seebeck coefficient as a function of temperature between 100 K and 320 K. (c) Power factor as a function of temperature between 100 K and 320 K.

The temperature-dependent electric properties were performed between 100 K and 320 K in a vacuum probe station. Figure 3(a) presents the four-probe electrical conductivity as a function of temperature. The electrical conductivity first decreases with decreasing temperature down to 205 K and increases with further decrease of temperature, forming a non-monotonous trend. The minimum conductivity at 205 K is 0.11 S/cm, and the maximum conductivity is 0.45 S/cm at 320 K.

Thermoelectrical measurement of the same device is presented in Fig. 3(b) as a function of temperature. The Seebeck coefficient is positive at room temperature, decreasing with temperature-drop down to 205 K. The further decrease of temperature results in a negative Seebeck coefficient, its amplitude increases at first and then decreases again at temperature close to 100 K. A clear sign change of the Seebeck coefficient is presented. The maximum amplitude of the measured Seebeck coefficient in the negative range is −92 μV/K at 176 K. The maximum of the Seebeck coefficient in the positive range is 537 μV/K at 320 K.

The feature of nonmonotonic temperature dependence of electrical conductivity and the sign change of Seebeck coefficient of SnSe nanoplates are observed for the first time and shared by multiple measured samples. One explanation of such a drastic change could be due to semiconductor-to-metal transition. On the other hand, such a phase transition of SnSe has not been predicted and is not consistent with our large Seebeck coefficient measured at low temperatures. The other possible reason for the sign change and the non-monotonous trend is the change of a majority of carriers that form bipolar thermoelectrical transport.

The bipolar transport indicates that both electrons and holes contribute to electrical and thermoelectrical properties at the same time.[35,36] The measured Seebeck coefficient is a combination of the negative Seebeck coefficient from the electrons and the positive Seebeck coefficient from the holes.[37,38] The sign change of the total Seebeck coefficient is determined by the proportion of the electron Seebeck coefficient and the hole Seebeck coefficient. The total Seebeck coefficient is expressed as[39,40]

$$S = \frac{S_{\rm e} n\mu_{\rm e} + S_{\rm h} p\mu_{\rm h}}{n\mu_{\rm e} + p\mu_{\rm h}}, \tag{1}$$

where the S is the total Seebeck coefficient; n and $\mu_{\rm e}$ are carrier concentration and mobility for electrons, respectively; p and $\mu_{\rm h}$ are carrier concentration and mobility for holes, respectively.

The electron and hole exist simultaneously inside the crystal. The previous theoretical calculation predicts that the bipolar transport is expected when bandgap decreases from 0.61 eV ($Pnma$) to 0.39 eV ($Cmcm$) at ∼800 K.[22] However, the theoretical calculated bandgap by Loa *et al.*[28] below room temperature shows that the $E_{\rm g}$ slightly changes from 0.84 eV at 100 K to 0.86 eV at 320 K. Thus, the $E_{\rm g}$ difference between 100 K and 320 K can be neglected when considering origin of the bipolar transport.

The fact that the sign of Seebeck coefficient changes from positive to negative means that the electron and hole concentration changes differently with temperature, which is related to the Fermi energy.[35,36] The transition from p-type to n-type with decreasing temperature suggests the move-

ment of the Fermi energy away from the valence band to the conduction band, which is caused by the decreased contribution from acceptors at lower temperature.[35,36] We can attribute the electrical conductivity and Seebeck coefficient bipolar transport to Fermi energy shifting caused by the different thermal generation electrons and holes at different temperatures. Our bipolar transport below room temperature is different from the bipolar transport previously investigated above room temperature.[22,41,42] To our best knowledge, this is the first time that the thermoelectrical bipolar transport has been investigated at 100 K–320 K, accompanied with a sign change of Seebeck coefficient[43,44] and nonmonotonic electrical conductivity trend.

The turnup point for the electrical conductivity and Seebeck coefficient is almost the same at about 205 K. The consistency makes it clear that the reason behind comes from the same mechanism. As the electrical conductivity and amplitude of Seebeck coefficient both increase with temperature above 228 K, there appears a unique feature against commonly observed different trends between electrical and thermoelectrical dependence. It is easy to reach the conclusion that the power factor ($\mathrm{PF} = \sigma S^2$) will keep increasing in this range. As shown in Fig. 3(c), the power factor increases with temperature above 228 K. The maximum power factor measured is $0.13\,\mu\mathrm{W\cdot cm^{-1}K^{-2}}$ at 320 K, whereas lower than the intrinsic bulk SnSe power factor due to the low electrical conductivity.

To further study the bipolar transport, a two-band model is used to calculate the Seebeck coefficient as a function of Fermi energy. When both electron and hole contribute to the Seebeck coefficient, the total S can be expressed as Eq. (1). The Seebeck coefficient can be expressed as[5]

$$S_\mathrm{e} = -\frac{k_\mathrm{B}}{e}\left\{\frac{\left(r_\mathrm{e}+\frac{5}{2}\right)F_{r_\mathrm{e}+\frac{3}{2}}(\eta_\mathrm{e})}{\left(r_\mathrm{e}+\frac{3}{2}\right)F_{r_\mathrm{e}+\frac{1}{2}}(\eta_\mathrm{e})}-\eta_\mathrm{e}\right\}, \tag{2}$$

$$S_\mathrm{h} = \frac{k_\mathrm{B}}{e}\left\{\frac{\left(r_\mathrm{h}+\frac{5}{2}\right)F_{r_\mathrm{h}+\frac{3}{2}}(\eta_\mathrm{h})}{\left(r_\mathrm{h}+\frac{3}{2}\right)F_{r_\mathrm{h}+\frac{1}{2}}(\eta_\mathrm{h})}-\eta_\mathrm{h}\right\}, \tag{3}$$

$$n = \frac{4\pi}{h^3}\left(2m_\mathrm{e}^* k_\mathrm{B}T\right)^{\frac{3}{2}}F_{\frac{1}{2}}(\eta_\mathrm{e}), \tag{4}$$

$$p = \frac{4\pi}{h^3}\left(2m_\mathrm{h}^* k_\mathrm{B}T\right)^{\frac{3}{2}}F_{\frac{1}{2}}(\eta_\mathrm{h}), \tag{5}$$

where $F_r(\eta) = \int_0^\infty \frac{x^r dx}{e^{(x-\eta)}+1}$ is the Fermi–Dirac integral of order r, both r_e and r_h are -0.5,[40] $\eta_\mathrm{e} = \frac{E_f}{k_\mathrm{B}T}$ and $\eta_\mathrm{h} = -\frac{E_f+E_\mathrm{g}}{k_\mathrm{B}T}$ are Fermi energies of electrons and holes; respectively; and k_B is the Boltzmann constant. The band gap E_g is 0.86 eV as reported; m_e^* and m_h^* are the effective masses of electron and hole and take the value of $0.13m_0$ and $0.14m_0$, respectively;[45] and h is Planck's constant.

Figure 4 shows the calculated Seebeck coefficient at 300 K as a function of $-E_f$ (as the sample at 300 K is p-type). The Seebeck coefficient is non-monotonic and changes from positive to negative with decreasing $-E_f$. The amplitude of the Seebeck coefficient first increases to the positive maximum, then decreases and crosses zero, and increases to the negative maximum, finally decreases close to zero, which is consistent with our bipolar transport. The non-monotonic and sign change in our calculation shows the similar bipolar transport behavior, which indicates electron's and hole's contribution should be both considered.[36] Thus, the non-monotonic relationship of the electrical conductivity and temperature together with the sign change of the Seebeck coefficient can be explained by the two-band transport model.

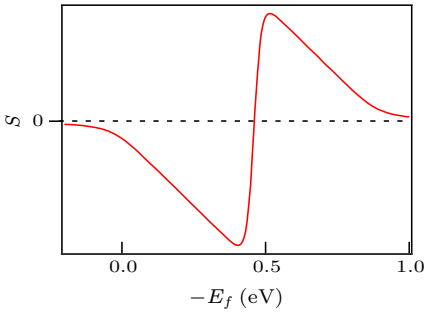

Fig. 4. Calculated Seebeck coefficient as a function of $-E_f$ at 300 K based on the two-band model.

In summary, the CVD synthesized SnSe nanoplates show an outstanding Seebeck coefficient, which is comparable to the intrinsic bulk SnSe. For the first time, low-temperature dependent electrical conductivity and Seebeck coefficient are shown, revealing a non-monotonic trend due to the bipolar transport of SnSe nanoplates. More interestingly, the Seebeck coefficient changes sign with temperature, which is caused by the Fermi level shifting due to the decreased contribution from accepters at lower temperature, described by the two-band model. Above 228 K, the electrical conductivity and the amplitude of the Seebeck coefficient increase simultaneously with temperature, leading to the same trend in power factor. Thus, the bipolar transport is non-negligible and can heavily affect the thermoelectric property of these materials.

References

[1] Snyder G J and Toberer E S 2008 *Nat. Mater.* **7** 105
[2] Nolas G S, Sharp J and Goldsmid H J 2001 Thermoelectrics: Basic Principles and New Materials Development (Berlin:

Springer)
[3] Rowe D M 1995 CRC Handbook of Thermoelectrics (Boca Raton: CRC Press)
[4] Hicks L D and Dresselhaus M S 1993 *Phys. Rev. B* **47** 16631
[5] Hicks L D and Dresselhaus M S 1993 *Phys. Rev. B* **47** 12727
[6] Dresselhaus M S, Chen G, Tang M Y, Yang R G, Lee H, Wang D Z, Ren Z F, Fleurial J P and Gogna P 2007 *Adv. Mater.* **19** 1043
[7] Fan P, Cai Z K, Zheng Z H et al 2011 *Acta Phys. Sin.* **60** 98402 (in Chinese)
[8] Feng J J, Zhu W and Deng Y 2018 *Chin. Phys. B* **27** 047210
[9] Morelli D T, Caillat T, Fleurial J P, Borshchevsky A, Vandersande J, Chen B and Uher C 1995 *Phys. Rev. B* **51** 9622
[10] Nolas G S, Morelli D T and Tritt T M 1999 *Annu. Rev. Mater. Sci.* **29** 89
[11] Lu T Q, Nan P F, Song S L, Zhu X Y, Zhao H Z and Deng Y 2018 *Chin. Phys. B* **27** 047207
[12] Xu K Q, Zeng H R, Yu H Z, Zhao K Y, Li G R, Song J Q, Shi X, Chen L D 2014 *Chin. Phys. Lett.* **31** 127201
[13] Wu D, Cao X H, Chen S Z, Tang L M, Feng Y X, Chen K Q and Zhou W X 2019 *J. Mater. Chem. A* **7** 19037
[14] Chen R, Lee J, Lee W and Li D 2019 *Chem. Rev.* **119** 9260
[15] Bell L E 2008 *Science* **321** 1457
[16] Kim J, Shim W and Lee W 2015 *J. Mater. Chem. C* **3** 11999
[17] Zhai J, Wang T, Wang H, Su W, Wang X, Chen T and Wang C 2018 *Chin. Phys. B* **27** 047306
[18] Chang C, Wu M, He D, Pei Y, Wu C F, Wu X, Yu H, Zhu F, Wang K, Chen Y, Huang L, Li J F, He J and Zhao L D 2018 *Science* **360** 778
[19] Zhao L D, Chang C, Tan G and Kanatzidis M G 2016 *Energy & Environ. Sci.* **9** 3044
[20] Shi W, Gao M, Wei J, Gao J, Fan C, Ashalley E, Li H and Wang Z 2018 *Adv. Sci. (Weinh)* **5** 1700602
[21] Chen Z G, Shi X, Zhao L D and Zou J 2018 *Prog. Mater. Sci.* **97** 283
[22] Zhao L D, Lo S H, Zhang Y, Sun H, Tan G, Uher C, Wolverton C, Dravid V P and Kanatzidis M G 2014 *Nature* **508** 373
[23] Guo R, Wang X, Kuang Y and Huang B 2015 *Phys. Rev. B* **92** 115202
[24] Duong A T, Nguyen V Q, Duvjir G, Duong V T, Kwon S, Song J Y, Lee J K, Lee J E, Park S, Min T, Lee J, Kim J and Cho S 2016 *Nat. Commun.* **7** 13713
[25] Poudel B, Hao Q, Ma Y, Lan Y, Minnich A, Yu B, Yan X, Wang D, Muto A, Vashaee D, Chen X, Liu J, Dresselhaus M S, Chen G and Ren Z 2008 *Science* **320** 634
[26] Biswas K, He J, Blum I D, Wu C I, Hogan T P, Seidman D N, Dravid V P and Kanatzidis M G 2012 *Nature* **489** 414
[27] Heremans J P, Dresselhaus M S, Bell L E and Morelli D T 2013 *Nat. Nanotechnol.* **8** 471
[28] Loa I, Popuri S R, Fortes A D and Bos J W G 2018 *Phys. Rev. Mater.* **2** 085405
[29] Pei T, Bao L, Ma R, Song S, Ge B, Wu L, Zhou Z, Wang G, Yang H, Li J, Gu C, Shen C, Du S and Gao H J 2016 *Adv. Electron. Mater.* **2** 1600292
[30] Brovman Y M, Small J P, Hu Y, Fang Y, Lieber C M and Kim P 2016 *J. Appl. Phys.* **119** 234304
[31] Small J P, Perez K M and Kim P 2003 *Phys. Rev. Lett.* **91** 256801
[32] Lee S, Yang F, Suh J, Yang S, Lee Y, Li G, Sung Choe H, Suslu A, Chen Y, Ko C, Park J, Liu K, Li J, Hippalgaonkar K, Urban J J, Tongay S and Wu J 2015 *Nat. Commun.* **6** 8573
[33] Tayari V, Senkovskiy B V, Rybkovskiy D, Ehlen N, Fedorov A, Chen C Y, Avila J, Asensio M, Perucchi A, di Pietro P, Yashina L, Fakih I, Hemsworth N, Petrescu M, Gervais G, Grüneis A and Szkopek T 2018 *Phys. Rev. B* **97** 045424
[34] Shi L, Li D, Yu C, Jang W, Kim D, Yao Z, Kim P and Majumdar A 2003 *J. Heat Transfer* **125** 881
[35] Afifi M A, Abdel-Aziz M M, Yahia I S, Fadel M and Wahab L A 2008 *J. Alloys Compd.* **455** 92
[36] Brahmi H, Neupane R, Xie L, Singh S, Yarali M, Katwal G, Chen S, Paulose M, Varghese O K and Mavrokefalos A 2018 *Nanoscale* **10** 3863
[37] Bejenari I and Kantser V 2008 *Phys. Rev. B* **78** 115322
[38] Goldsmid H J 2014 *Materials* **7** 2577
[39] Zhang J, Feng X, Xu Y, Guo M, Zhang Z, Ou Y, Feng Y, Li K, Zhang H, Wang L, Chen X, Gan Z, Zhang S C, He K, Ma X, Xue Q K and Wang Y 2015 *Phys. Rev. B* **91**
[40] Mavrokefalos A, Moore A L, Pettes M T, Shi L, Wang W and Li X 2009 *J. Appl. Phys.* **105** 104318
[41] Chen C L, Wang H, Chen Y Y, Day T and Snyder G J 2014 *J. Mater. Chem. A* **2** 11171
[42] Ibrahim D, Vaney J B, Sassi S, Candolfi C, Ohorodniichuk V, Levinsky P, Semprimoschnig C, Dauscher A and Lenoir B 2017 *Appl. Phys. Lett.* **110** 032103
[43] Wang S, Hui S, Peng K, Bailey T P, Liu W, Yan Y, Zhou X, Tang X and Uher C 2018 *Appl. Phys. Lett.* **112** 142102
[44] Hernandez J A, Ruiz A, Fonseca L F, Pettes M T, Jose-Yacaman M and Benitez A 2018 *Sci. Rep.* **8** 11966
[45] Zhou M, Chen X, Li M and Du A 2017 *J. Mater. Chem. C* **5** 1247